

Available online at www.sciencedirect.com

ScienceDirect

journal homepage: www.elsevier.com/locate/AJPS

Original Research Paper

The design and synthesis of dextran-doxorubicin prodrug-based pH-sensitive drug delivery system for improving chemotherapy efficacy



Xiaoli Zhang^{a,1}, Tian Zhang^{b,c,1}, Xianbin Ma^{b,c}, Yajun Wang^{b,c}, Yi Lu^{b,c}, Die Jia^{b,c}, Xiaohua Huang^d, Jiucun Chen^b, Zhigang Xu^{b,c,d,*}, Feiqiu Wen^{a,**}

^aDepartment of Hematology and Oncology, Shenzhen Children's Hospital, Shenzhen 518038, China

^bSchool of Materials and Energy, Southwest University, Chongqing 400715, China

^cChongqing Engineering Research Center for Micro-Nano Biomedical Materials and Devices, Chongqing 400715, China

^dGuangan Changming Research Institute for Advanced Industrial Technology, Guangan 638500, China

ARTICLE INFO

Article history:

Received 26 June 2019

Revised 2 September 2019

Accepted 10 October 2019

Available online 6 November 2019

Keywords:

Dextran

Chemotherapy

Prodrug

Tumor acidic microenvironment

Controlled release

ABSTRACT

Tumor cells show acidic conditions compared with normal cells, which further inspires scientist to build nanocarrier responsive to tumor microenvironment (TME) for enhancing tumor therapeutic efficacy. Here, we report a pH-sensitive and biocompatible polyprodrug based on dextran-doxorubicin (DOX) prodrug (DOXDT) for enhanced chemotherapy. High-density DOX component was covalently decorated on the nanocarrier and the drug molecules could be effectively released in the acidic tumor tissue/cells, improving chemotherapy efficacy. Specifically, a dextran-based copolymer was preliminarily prepared by one-step atom transfer radical polymerization (ATRP); then DOX was conjugated on the copolymer component via pH-responsive hydrazone bond. The structure of DOXDT can be well-controlled. The resulting DOXDT was able to further self-assemble into nanoscale micelles with a hydration diameter of about 32.4 nm, which presented excellent micellar stability. Compared to lipid-based drug delivery system, the DOXDT prodrug showed higher drug load capacity up to 23.6%. In addition, excellent stability and smaller size of the nanocarrier contributed to better tissue permeability and tumor suppressive effects *in vivo*. Hence, this amphipathic DOXDT prodrug is promising in the development of translational DOX formulations, which would be widely applied in cancer therapy.

© 2019 Shenyang Pharmaceutical University. Published by Elsevier B.V.

This is an open access article under the CC BY-NC-ND license.

(<http://creativecommons.org/licenses/by-nc-nd/4.0/>)

* Corresponding author. School of Materials and Energy, Southwest University, Chongqing 400715, China Tel.: +86 23 68253792.

** Corresponding author. Department of Hematology and Oncology, Shenzhen Children's Hospital, Shenzhen 518038, China Tel.: +86 755 83009888.

E-mail addresses: zgxu@swu.edu.cn (Z.G. Xu), fwen62@163.com (F.Q. Wen).

¹ These authors contributed equally to this work.

Peer review under responsibility of Shenyang Pharmaceutical University.

1. Introduction

In recent decades, cancer has been reported as an important and major cause of morbidity and mortality in every regions of the world [1]. Chemotherapy, as one of the most common cancer therapeutic methods, have drawn increasing attentions. Limited water solubility, nonspecific cytotoxicity, and undesirable adverse effects of traditional chemotherapy drugs lead to poor circulation performance and low tumor tissue-selective accumulation [2–7]. The clinical applications of these chemotherapy were further restricted since there was no feasible method for delivering drugs in solid tumor [8]. Hence, stimuli-responsive drug delivery systems [9–11] have been developed gradually for improving the efficacy of anti-cancer drugs [12]. Several important features of tumor microenvironment, such as low pH value, hypoxia, high glutathione (GSH) concentration, high levels of reactive oxygen species (ROS), unique enzymes, and high adenosine triphosphate (ATP) etc. [13,14], have been utilized for designing selective and smart drug-delivery strategies [15,16]. Currently, drug has been linked on an amphipathic polymer with the specific stimuli site by covalent bonding which dissociated in tumor microenvironment but not in normal tissues, presenting good bio-safety *in vivo*. And the prodrug can be delivered to the solid tumor because of enhanced permeability and retention (EPR) effect, which was also called passive targeting [17–19]. Thus, the chemotherapy effect can be improved.

Several nanoparticle-based drug delivery systems have been developed to improve the insufficient therapeutic of traditional chemotherapy and address the challenges of cancer treatment, including polymeric liposomes and micelles [20–26], small molecules prodrug [27–29] and inorganic delivery systems [30–33] et al. Compared to lipid, stimuli-responsive polymer-based drug-delivery systems exhibited stable structures and selective drug release for cancer therapy [34]. However, the challenges are how to realize the precise control of drug release and overcome the complicated biology of the intratumoral microenvironment [35]. Generally, the controllable release of drug in tumor can be realized by linking the drug with stimulate-sensitive chemical bonds, such as hydrazone bond [36], disulfide bond [37], thioketal [38] etc. Furthermore, polymeric drug can be self-assembled into nanoscale micelles in aqueous solution. The EPR effects can be realized to enhance tumor therapeutic efficacy with minimal side effects.

As a kind of polysaccharide, dextran (DEX) shows good water solubility, facile functionalization and indigestibility because of abundant hydroxyl groups. These advantages endow DEX as an ideal candidate for construction of DEX-based nanomedicine [39,40], and which enhanced the poor water solubility of drugs and delivery efficiency, producing an improved therapeutic effect. Thus, DEX had excellent potential for clinical applications. Hence, we have prepared a custom-designed DEX-P(OEGMA-co-MGMA) (DPP) polymer by one-step ATRP (Scheme 1). Then the doxorubicin (DOX) molecules were grafted on DEX skeleton through acid-activated hydrazone bond, producing dextran-DOX prodrug (DOXDT). The special structure design of DOXDT

prodrug realized controllable release of drug in acidic tumor environment. This block copolymer consisted of poly-OEGMA monomer as the hydrophilic layer for adjusting the hydrophilia of resulting DOXDT. The resulting DOXDT prodrug can be formed into stable micelles in water medium and showed improved tumor penetration, excellent *in vivo* blood compatibility and biodistribution, leading to an improved therapeutic efficacy.

2. Materials and methods

2.1. Materials

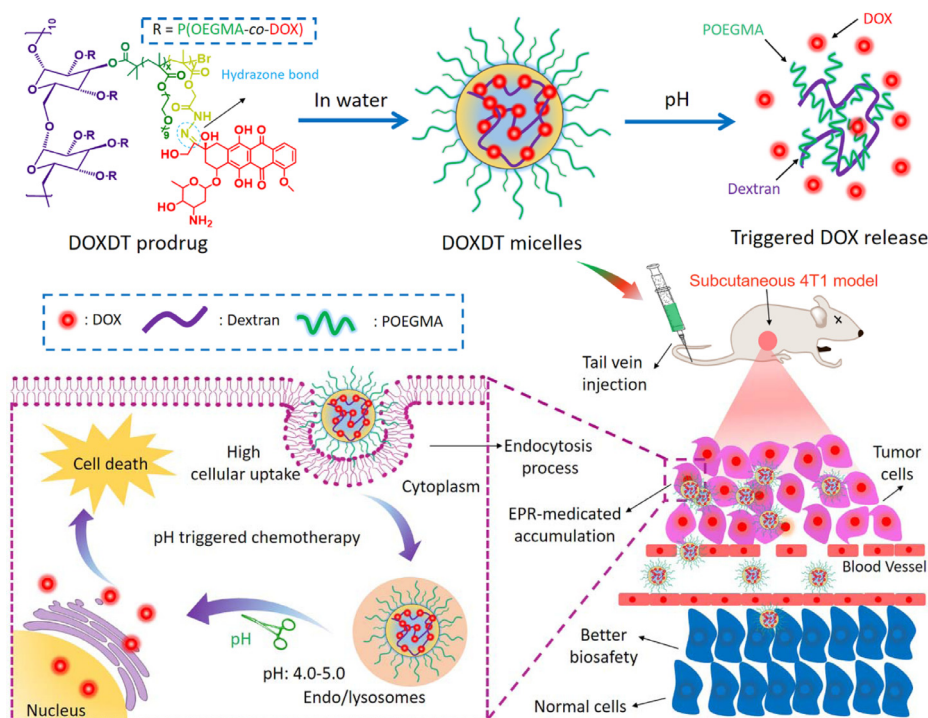
All chemical agents including Dextran (DEX, Mw 3500 Da), tris(2-dimethylaminoethyl)-amine (Me₆TREN), poly (ethylene glycol) methyl ether methacrylate (OEGMA), hydrazine hydrate and anhydrous solvents were obtained from Sigma-Aldrich (USA). Doxorubicin hydrochloride (DOX•HCl) and other analytical solvent were supplied by Adamas-beta (China). 1,2-distearoyl-sn-glycero-3-phosphoethanolamine-N-[methoxy(poly(ethylene glycol))-2000] (DSPE-mPEG2000) was obtained from A.V.T Pharmaceutical Co., Ltd. (Shanghai, China). Biological agents including 3-(4, 5-dimethylthiazol-2-yl)-2,5-diphenyltetrazolium bromide (MTT), Alexa Fluor® 488 phalloidin (AF-488), Lyso-Tracker Green dye and Cy5-NHS were purchased from Life Technologies (USA). TdT-mediated dUTP Nick-End Labeling (TUNEL) apoptosis assay Kit was supplied by Beyotime Biotechnology (China).

2.2. Synthesis of DEX-P(OEGMA-co-MGMA) polymer

The methyl glycolate methacrylate (MGMA) and DEX-Br were synthesized according to previous report [41,43]. The DEX-P(OEGMA-co-MGMA) (DPP) copolymer was prepared by one-step ATRP. Under argon protection, DEX-Br (28.3 mg), OEGMA (160 mg), MGMA (25.5 mg) and CuBr (15.6 mg) were all dissolved into mixed solution of equal volume N,N-Dimethylformamide (DMF) and dimethylsulfoxide (DMSO) in a Schlenk tube. After an oxygen removing process was carried out using liquid nitrogen, adding Me₆TREN (46 μl) and then stirring for 24 h at 25 °C. The final mixture was purified with cold diethyl ether three times. The product of DEX-P(OEGMA-co-MGMA) was obtained. The ¹H NMR analysis (Bruker AV 600 NMR) was performed to characterize the chemical structure and composition of final product. Gel permeation chromatography with Agilent 1260 pump and refractive index detector (GPC, Agilent 1260, USA) was applied to trace the polymerization results.

2.3. Synthesis of DOXDT prodrug

The DEX-P(OEGMA-co-MGMA) copolymer reacted with hydrazine hydrate for 12 h, then a dialysis method was used to remove unreacted agents, resulting in a product of DPP-hydrazide after the freeze-drying treatment. Next, 120 mg of DPP-hydrazide and 40 mg of DOX•HCl dissolved in a mixed solution of 2 ml DMF and 1 ml methanol at 25 °C, then two drops of trifluoroacetic acid (TFA) were added. The



Scheme 1 – The synthetic route of DOXDT micelles, pH-sensitive release of DOX drug, EPR-mediated drug accumulation and cell internalization, and the mechanism of cancer cell death.

mixture was then stirred at room temperature for more than 36 h and dialyzed against methanol adequately. The product DOXDT was obtained by vacuum. The ^1H NMR analysis was performed to characterize the chemical structure and composition of DOXDT prodrug.

2.4. Preparation of DOXDT micelles

Typically, 2 ml DMF solution contained 10 mg DOXDT was slowly added dropwise in 5 ml of water under sonication for 0.5 h. Then, above solution was dialyzed against water for 48 h. Finally, the DOXDT micelles were obtained. The Lip@DOX was also prepared to compare the *in vivo* tumor therapeutic effects [44]. Briefly, 2 ml of DOX·HCl solution in DMF (1 mg/ml) were added into 5 ml of DSPE-mPEG2000 water solution (2 mg/ml) under sonication, and then a dialysis process of Lip@DOX liposomes was similar to the preparation method of DOXDT micelles. The morphology of DOXDT micelles was demonstrated with transmission electron microscopy (TEM, JEM-2100, Japan) and the size was measured with dynamic light scattering (DLS, Nano ZS90, Malvern, UK). The absorption peak of DOXDT was detected with UV-vis spectrophotometer (UV-2550, Shimadzu, Japan) at 488 nm and the maximum fluorescence (FL) emission was determined with fluorophotometer (RF-5301 PC, Shimadzu, Japan) at 560 nm.

2.5. *In vitro* DOX release of the DOXDT micelles

The release profile of DOXDT micelles at different pH values were detected with a dialysis method (MW 3500 Da) under

shaking at 37 °C. Typically, 1 ml of micelles solution (500 µg/ml) was immersed in 80 ml of phosphate buffer saline (PBS) with various pH media. The released medium was sampled at different time point and equal volume of fresh medium was added. Then, the concentration of DOX in the medium was determined based on the standard curve of DOX at emission wavelength of 560 nm.

2.6. Cell cultures

Mouse breast cancer cell line (4T1) and human cervical cancer cell line (HeLa) were all cultured in Dulbecco's modified eagle's medium (DMEM) medium supplemented with 10% fetal bovine serum (FBS) and 1% penicillin/streptomycin (PS). The cells were cultured at 37 °C in an incubator with 5% CO_2 humid atmosphere.

2.7. *In vitro* cytotoxicity of the DOXDT micelles

In vitro cytotoxicity of DOXDT micelles were evaluated with HeLa and 4T1 cells. Firstly, cells were added in a 96-well plate at a density of 10^4 cells/well and incubated for 12 h in an incubator. Then the old DMEM was replaced with different treatment for a 72 h incubation. Then 100 µl of MTT agent was added (0.5 mg/ml) after removing DMEM solution. After 4 h, the supernatant was removed, and the formazan was dissolved with 100 µl of DMSO. The absorbance at 570 nm was detected with microplate reader for calculating the cell viability (Tecan Infinite Spark-10 M, Switzerland).

2.8. Live/dead assay

The *in vitro* live/dead study was performed to further evaluate the cell apoptosis induced by DOXDT prodrug. Cells were cultivated overnight in 12-well plate with the cell density of 1.5×10^5 HeLa cells per well. The old medium was replaced by 1 ml fresh medium containing free DOX or DOXDT (DOX concentration: 20 $\mu\text{g}/\text{ml}$) for 24 h. Next, the cells were stained with a Live/Dead kit for 20 min and the fluorescence images were observed with the fluorescence microscope (Olympus IX71).

2.9. Cellular uptake

Cells were cultivated overnight in 8-well plate with cell density of 2.0×10^4 HeLa cells/well. Then the cells were incubated with DMEM containing free DOX or DOXDT (equivalent DOX concentration: 20 $\mu\text{g}/\text{ml}$) for 2 and 6 h. Next, formalin solution, BSA and Triton X-100 were added in sequence. Cytoskeleton and nucleus were stained with AF488 phalloidin and 4',6-diamidino-2-phenylindole (DAPI) respectively. The fluorescence images of the cells were captured with Confocal Laser Scanning Microscopy (CLSM, Zeiss 800).

To further study the cellular uptake process of DOXDT, cells were cultivated overnight in 12-well plate with the cell density of 1.0×10^5 HeLa cells per well. After the treatment with DMEM containing free DOX or DOXDT solution at different time-point, the cellular uptake results of DOXDT were obtained by flow cytometry (NovoCyte 2060R, USA).

2.10. In vitro lysosome co-localization

Cells were cultivated overnight in 8-well plate with cell density of 2.0×10^4 HeLa cells per well. Then, the cells were incubated with DMEM containing free DOX or DOXDT (equivalent DOX concentration: 20 $\mu\text{g}/\text{ml}$) for 2 and 6 h. After the treatment, the cells were stained with Lyso-Tracker Green dye for 1 h. Finally, the cells were washed three times with PBS and the fluorescence images were captured with CLSM.

2.11. Penetration of multicellular spheroids (MCS)

MCS of 4T1 cells were applied to simulate the solid tumor for evaluating the deep penetration effect of DOXDT micelles. The MCS was treated with DMEM containing Lip@DOX and DOXDT (equivalent DOX concentration: 20 $\mu\text{g}/\text{ml}$) for 6 h, respectively. Then the MCS were washed three times by PBS and observed with CLSM.

2.12. Animal models

All animal experiments were conducted according to the animal experiments guidelines reviewed and approved by the University Committee on Use and Care of Animals (UCUCA) at Southwest University. Balb/c female nude mice (Balb/C, weighed 20–25 g, for biodistribution and therapeutic treatment) and Kunming female mice (KM, weighed 20–25 g, for routine blood test) were supplied by Chongqing Teng

xin Biological Technology Co. Ltd. (Chongqing, China). 200 μl of 4T1 cells (5×10^6 cells) were injected in right armpit of nude mice for establishing the tumor-bearing animal models. Experiments began after the tumors were grown to about 100 mm^3 .

2.13. Blood routine

The KM mice were injected with 200 μl of saline, free DOX, Lip@DOX and DOXDT, respectively (equivalent DOX concentration: 5 mg/kg) through tail veins. After 1 and 7 d, the blood was collected from the orbit of each mouse. The indicators in blood was analyzed with a hematology analyzer (Mindray BC-2600Vet), and experiment results including white blood cell count (WBC), lymphocyte ratio (LYM), hemoglobin concentration (HGB), hematocrit (HCT), mean corpuscular hemoglobin concentration (MCHC), red blood cell count (RBC), mean platelet volume (MPV) variation coefficient of red blood cell distribution width (RDW) and platelets (PTL) were collected.

2.14. In vivo fluorescence imaging

The Balb/C mice bearing tumor formed by 4T1 cells were injected with Cy5, Cy5-labeled Lip@DOX and Cy5-labeled DOXDT (Cy5: 1.0 mg/ml , 200 μl) were injected through tail veins. Near-infrared imaging of the mice were collected after 24 h by NIR imaging system (PerkinElmer IVIS Lumina Kinetic Series III NIR imaging system), including tumors and major organs (heart, liver, spleen, lung and kidney).

2.15. In vivo therapeutic assay

Four groups of Balb/C mice bearing 4T1 tumor ($n = 5$ per group) were injected with saline, free DOX, Lip@DOX and DOXDT (equivalent DOX concentration: 5 mg/kg) through intravenous injection. The tumor volume and body weight were recorded every day during 14 d of treatment. The tumor volume was calculated using the formula:

$$\text{Volume (mm}^3\text{)} = \text{Length (mm)} \times \text{Width}^2 \text{(mm}^2\text{)} \times 0.5.$$

After the treatment, the mice were sacrificed. The major organs including (kidney, lung, spleen, liver and heart) and tumors were removed, sliced, and embedded in paraffin. The slices of all samples were treated using hematoxylin and eosin (H&E). In addition, the slices of tumors were stained with TUNEL to study the apoptosis of tumor cells. The fluorescence of DOX was observed in some slices of tumors stained with DAPI, and it aimed to study the permeability of DOXDT prodrug for solid tumor. All the fluorescence images of the slices were obtained by fluorescence microscope (IX 73, Olympus).

3. Results and discussion

3.1. Synthesis and characterizations of DPP polymer and DOXDT prodrug

The DEX-P (OEGMA-co-MGMA) (DPP) copolymer was prepared with one-step ATRP reaction with DEX-Br as the initiator.

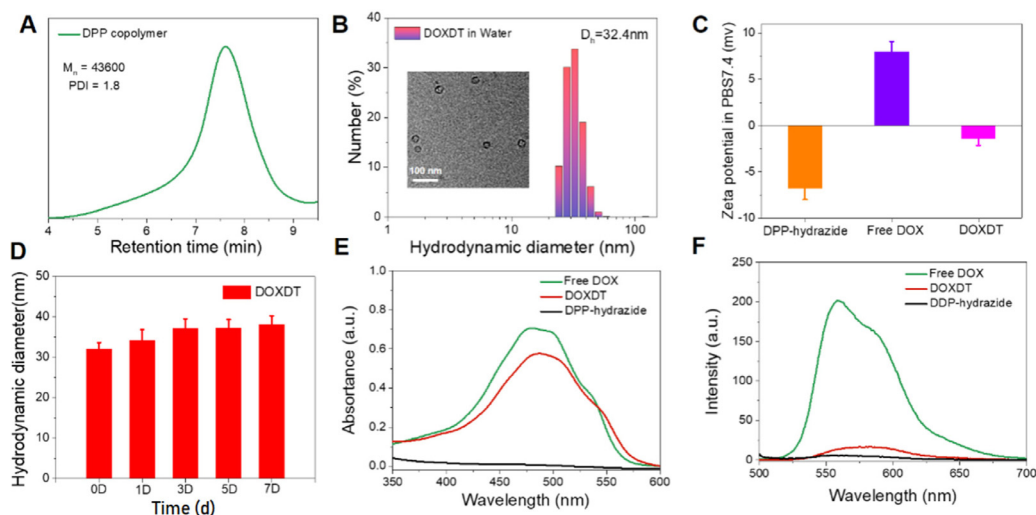


Fig. 1 – The characterization of DOXDT. (A) The GPC result of DOXDT micelles. (B) The DLS result and TEM image of DOXDT micelles formed in water. (C) The zeta potential of DPP-hydrazide, free DOX and DOXDT. (D) The stability of DOXDT micelles in water for 7 d, and data were expressed as mean \pm SD ($n = 3$). UV-vis absorption (E) and fluorescence spectra (F) of DPP-hydrazide, free DOX and DOXDT.

In DEX molecules, about 72% of hydroxyl groups were converted into reaction-sites. Specifically, the copolymers of DPP were prepared by the reaction between DEX-Br with OEGMA and MGMA monomer. DOXDT was prepared through two steps. Firstly, DPP reacted with hydrazine hydrate to get intermediate product DPP-hydrazide. Then DPP-hydrazide reacted with DOX to obtain DOXDT prodrug. The synthesis routes of DPP and DOXDT were shown (Fig. S1). The chemical structure and composition of DPP and DOXDT were performed with ^1H NMR analysis (Fig. S2). The characteristic signals of OEGMA block were located at peak b (3.64 ppm) corresponding to methylene protons. While for MGMA block, the characteristic signal located at 4.71 ppm (peak d) was related to the methylene protons close to the ester moiety. These signals indicated the successful polymerization of the OEGMA and MGMA monomer with the DEX-Br initiator. And the disappearance of peak at 3.76 ppm (peak c) demonstrated the successful replacement of methoxy group by the hydrazine group, and two signals at peak e and peak f further confirmed the successful synthesis of the DOXDT prodrug. The polymerization results were traced with gel permeation chromatography (Fig. 1A). For the DPP copolymers, the number-average molecular weight (M_n) was 43,600 g/mol, and polymer dispersity index (PDI) was about 1.8 (Fig. 1A).

3.2. The characterization of DOXDT micelles

Due to amphiphilic structure-based dextran polyprodrug, the DOXDT showed the potential to form unimolecular micelles in water medium [41]. To assess the DOXDT solution in water, the morphology and size distribution of DOXDT micelles were demonstrated with TEM and DLS technologies, respectively. Specifically, the average diameter of spherical micelles was about 26.90 ± 2.01 nm by TEM (Fig. 1B Inset). However, the average diameter of DOXDT micelles was about 32.4 nm

by DLS (Fig. 1B). Notably, the size of DOXDT micelles in water could remain stable for 7 d, which indicated the good structural stability (Fig. 1D). To confirm the formation of unimolecular micelles, we further measured the DLS results of DOXDT solution in DMF, which is a good solvent for both chains of DOXDT. More exactly, DOXDT could exist as unimolecular micelles in water. As showed in Fig. S3, the average diameter of DOXDT micelles in DMF was about 33.65 nm by DLS, which is almost identical to the in water. These results collectively demonstrated the formation of DOXDT unimolecular micelles in water [42].

Additionally, the zeta potential of DPP-hydrazide and free DOX were -6.842 mV and 8.066 mV, respectively. While for the DOXDT micelles was generally neutral in PBS (pH = 7.4), with zeta potential of -1.456 mV, which would be favorable for blood circulation (Fig. 1C). The optical properties of DOXDT micelles in water were characterized (Fig. 1E and 1F). The absorption peak of DOXDT and the maximum fluorescence emission intensity of DOXDT micelles can be observed at 488 nm and 560 nm, which were close to the DOX.

3.3. pH-sensitive DOX release and in vitro cytotoxicity

According to the standard curve of fluorescence intensity against DOX concentration, the drug loading content (LC%) of DOXDT prodrug was 23.6% (w/w). The release behavior of DOX from DOXDT was analyzed with dialysis method. The accumulative release amount of DOX was up to 72.43% at pH 5.0, while 28.97% at pH 6.8 or only 15.71% at pH 7.4 (Fig. 2A). The accumulative DOX release at pH 5.0 was higher than that of at pH 6.8 and 7.4. As showed in Fig. 2B, the reasonable release mechanism was attributed by the pH-sensitive hydrazine bond, which could be dissociated under acidic tumor microenvironment [36]. In conclusion, acidic environment-sensitive DOXDT-based delivery system could lead to selective delivery. On the contrary, the release rate

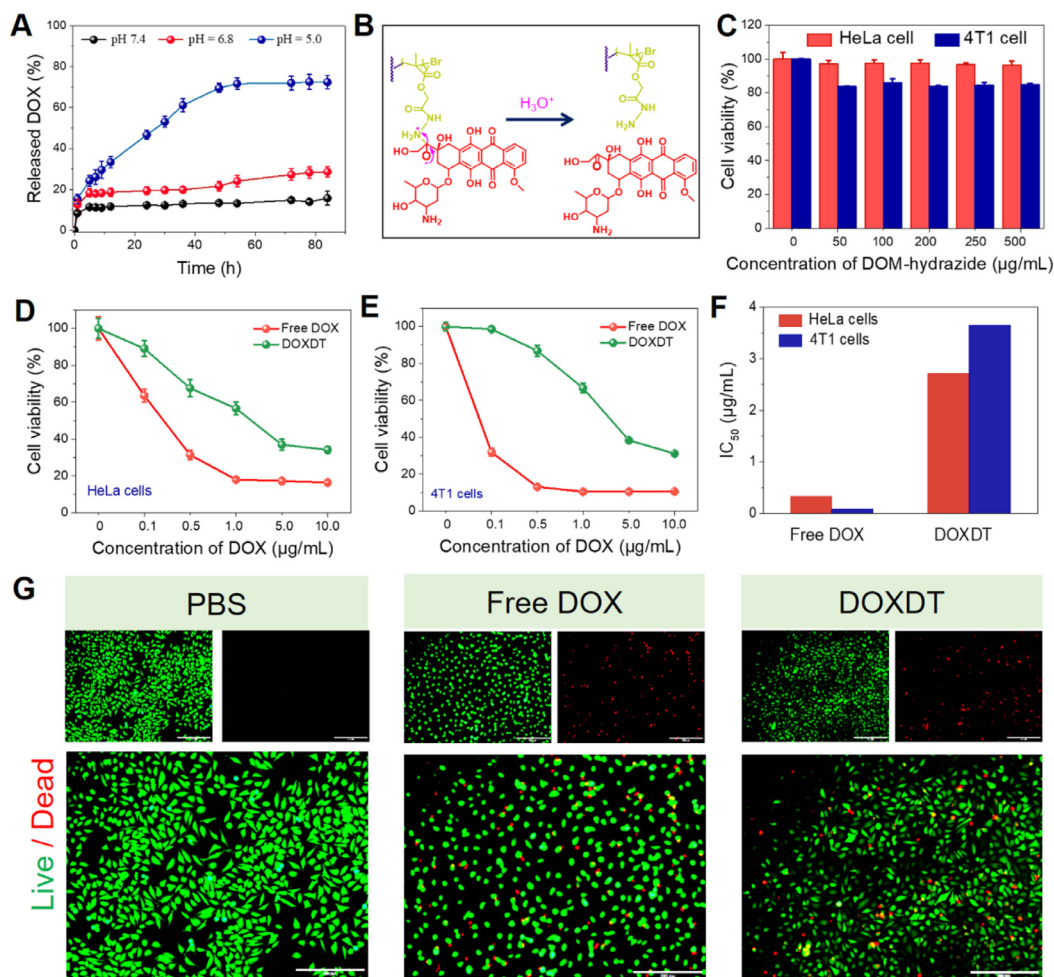


Fig. 2 – The performances of DOXDT. (A) Acidity-activated DOX release profiles of DOXDT. (B) Mechanism of pH-sensitive DOX release from DOXDT prodrug. Cell viability of HeLa and 4T1 cells (C) after treating with different concentrations of DPP-hydrazide for 72 h. Cell viability of HeLa (D) and 4T1 cells (E) after treating with different concentrations of free DOX and DOXDT for 72 h. Data were expressed as mean \pm SD ($n = 3$). (F) Half maximal inhibitory concentration (IC_{50}) of free DOX and DOXDT for HeLa and 4T1 cells. (G) Live (Fluorescein diacetate, green)/Dead (propidium iodide, red) fluorescence staining of HeLa cells treated with PBS, free DOX, DOXDT (the concentration of DOX: 20 $\mu\text{g}/\text{ml}$) for 24 h. Scale bars: 200 μm . (For interpretation of the references to colour in this figure legend, the reader is referred to the web version of this article.)

of DOX was decreased at neural pH in normal tissues, thus minimizing the side effects.

In addition, the cytotoxicity of DOXDT against cancer cells was performed on both 4T1 and HeLa cells for evaluating the tumor inhibiting effects *in vitro*. Specifically, the cells were treated with different concentrations of DPP-hydrazide (0 to 500 $\mu\text{g}/\text{ml}$). As showed in the Fig. 2C, about 90% of HeLa cells and about 80% 4T1 cells were alive after treating with the maximal concentration for 72 h, indicating no obvious cytotoxicity. The results proved the good *in vitro* biosafety of the DOXDT prodrug.

Cell viability of HeLa and 4T1 cells was significantly decreased when the DOX concentration of DOXDT was ranged from 0 to 10 $\mu\text{g}/\text{ml}$ (Fig. 2D and 2E). Specifically, the viable HeLa and 4T1 cells were dramatically reduced to only 30% after treating with DOXDT for 72 h. Tumor-specific cytotoxicity was owe to the acidic tumor microenvironment-triggered hydrazine bond cleavage, which lead to the controlled DOX

release from DOXDT. The cytotoxicity of two cell lines treated with free DOX showed a stronger toxicity than that of DOXDT group, which was suggested to be caused by the small size and non-selective cytotoxicity of free DOX. The results were further supported with the half maximal inhibitory concentration (IC_{50}) of DOXDT and free DOX for HeLa and 4T1 cells (Fig. 2F). Additionally, the cell apoptosis of DOXDT prodrug was further evaluated with the Live/Dead assay (Fig. 2G). The group treated with DOXDT exhibited a similar proportion of red and green fluorescence compared to that of treated with free DOX, suggesting its good therapeutic effects against tumor cells.

3.4. *In vitro* cellular uptake and lysosome co-localization

Usually, a nanoparticle-based drug delivery system showed similar cell uptake behavior for different tumor cells [45].

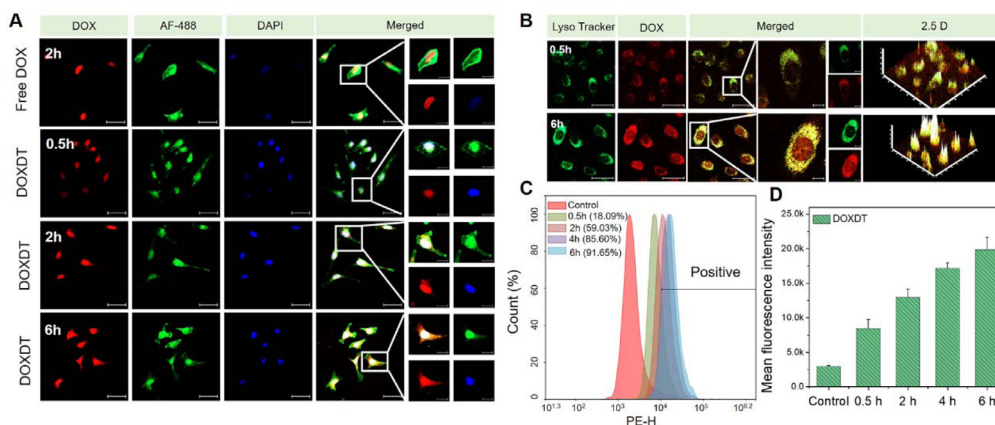


Fig. 3 – Cellular uptake and localization of DOXDT. (A) CLSM images showed the distribution of DOX in HeLa cells after treating with free DOX for 2 h or DOXDT for 0.5, 2 and 6 h. **(B)** CLSM images showed the HeLa cells after treating with DOXDT for 0.5 and 6 h, and then staining with Lyso-Tracker Green dye. Scale bars: 50 μ m. **(C)** The HeLa cells were treated with DOXDT for 0.5, 2, 4 and 6 h and cellular uptake was analyzed with flow cytometry. **(D)** The mean fluorescence intensity of HeLa cells after incubating with DOXDT micelles for different time.

Therefore, the cell uptake behavior of DOXDT was studied in HeLa cells with CLSM. Specifically, the nuclei and cytoskeleton of cells were stained with DAPI (blue) and AF488 (green), respectively. Strong red fluorescence of DOX could be observed at the nuclei after treating with free DOX for 2 h, indicating a rapid internalization process of free DOX (Fig. 3A). The red fluorescence intensity of DOX was generally increased with the incubation time. The phenomenon might be resulted from the time-dependent drug release behavior of DOXDT micelles in acidic environment of cancer cells. The magnified image further demonstrated that drug accumulation in the nuclear region was gradually increased over time.

The cellular uptake efficiency of DOXDT micelles in HeLa cells was quantitatively evaluated. HeLa cells were treated with DOXDT micelles for different time. As showed in Fig. 3C, 3D and S4, the uptake rate of DOXDT reached up to 91.65% after treating for 6 h. The average fluorescence intensity of DOX was gradually increased, demonstrating the remarkable cellular uptake capability of DOXDT micelles.

The cell internalization pathway of DOXDT was determined with CLSM (Fig. 3B). HeLa cells were treated with DOXDT for 0.5 and 6 h, respectively, and lysosome of cells was stained with Lyso-Tracker Green dye. The red fluorescence intensity of DOX was increased with time, indicating the micelles were successful localized in lysosomes after 6 h of incubation.

3.5. Penetration study in 4T1 multicellular spheroids (MCS)

The 4T1 MCS was applied to simulate solid tumor for studying the permeability of DOXDT micelles [46]. The results were observed by CLSM Z-stack scanning with a 10 μ m interval between each slice, and the slice with the strongest fluorescence intensity was regarded as 0 μ m. As shown in Fig. 4A, red fluorescence intensity of MCS treated with DOXDT was obviously stronger than that of MCS treated with Lip@DOX at 0 μ m. Furthermore, at the 60 μ m scanning

depth of MCSs, the red fluorescence signals of DOXDT group showed a stronger signal in comparison of Lip@DOX group. As showed in Fig. S5, the average diameter of Lip@DOX was about 26.32 nm, which is slightly smaller than that of DOXDT in water. Therefore, the micellar size was not the dominant factor for the enhanced permeability of DOXDT. However, compared with Lip@DOX, DOXDT showed a nature of unimolecular micelles, which could maintain a stronger micellar stability of DOXDT than that of Lip@DOX under a very lower concentration or complex tumor microenvironment. The nano-sized micellar state further endow DOXDT with an improved permeability and retention [42,47].

3.6. In vivo blood compatibility and biodistribution

KM mice was applied as models for studying the blood compatibility of DOXDT micelles *in vivo* using a hematology analyzer. A series of indicators including WBC, LYM, HGB, RBC, HCT, MCHC, MPV, RDW and PLT were recorded and showed in Fig. 4B, the levels of routine blood indices were all within the normal ranges, confirming the good *in vivo* blood compatibility of DOXDT micelles.

Additionally, Balb/C mice bearing 4T1 tumors were applied as models to trace the biodistribution of DOXDT micelles *in vivo*. Cy5-NHS fluorescent dye was applied to modify the prodrugs by the chemical reaction between NHS group in Cy5-NHS dye and amino group in prodrug for further near-infrared imaging. Specifically, free Cy5, Cy5-labelled Lip@DOX and Cy5-labelled DOXDT were injected into the mice. As shown in Fig. 4C, the group treated with free Cy5 showed almost no near-infrared fluorescence in the site of tumor. The free Cy5 could be easily eliminated from blood 24 h after intravenous injection. In contrast, the mice injected with Cy5-labelled micelles showed quite strong fluorescence signal. To our surprise, the group treated with DOXDT exhibited stronger fluorescence than that of Lip@DOX group, which may benefit from high tumor permeability and retention of prodrug compared to liposome. These results further

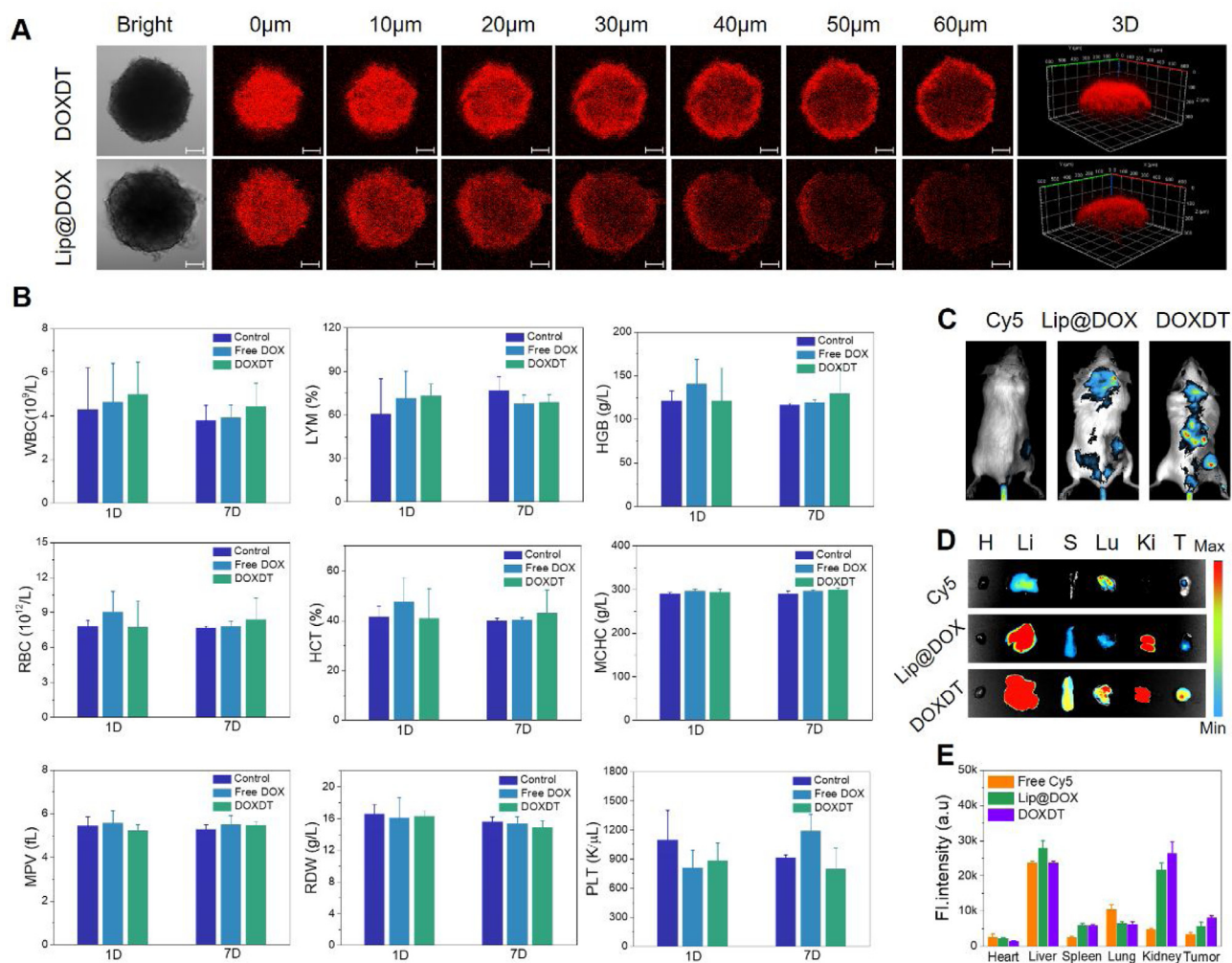


Fig. 4 – The tumor penetration and blood biocompatibility of DOXDT. (A) CLMS images of 4T1 MCS after treating with Lip@DOX and DOXDT for 6 h. Scale bars: 100 μ m. (B) The complete blood indices of KM mice after the injection of PBS, free DOX and Lip@DOX and DOXDT (DOX dosage: 5 mg/kg), respectively, at Day 1 and Day 7. (C) Fluorescence images of Balb/C mice, (D) the tumors and major organs removed from mice, including heart (H), liver (L), spleen (S), lung (Lu), kidney (K) and tumor (T), and the quantitative comparison of the ex vivo fluorescence distribution (E) after the injection of free Cy5, Cy5-labeled Lip@DOX and Cy5-labeled DOXDT after 24 h. Data were expressed as mean \pm SD ($n = 3$).

confirmed that the prodrug could be released based on acidity and accumulated in tumor tissues, thus enhancing the tumor therapy efficiency. Furthermore, the tumors and major organs (heart, liver, spleen, lung and kidney) were removed for further evaluating the selective drug accumulation (Fig. 4D). The corresponding fluorescence intensity was quantified (Fig. 4E). The fluorescence intensity of tumor in DOXDT treated group was significantly stronger than that of in Lip@DOX treated group. These phenomena might be resulted from the smaller size of DOXDT prodrug compared to Lip@DOX.

3.7. *In vivo* tumor therapeutic effects

Balb/C mice bearing 4T1 tumors were selected to evaluate the tumor inhibitory effects of DOXDT prodrug *in vivo*. Specifically, tumor-bearing mice were treated with saline,

free DOX, Lip@DOX and DOXDT (DOX dosage: 5 mg/kg) every 3 d. As showed in Fig. 5A, the tumor volume of mice in PBS group was rapidly increased from 139.74 to 1376.35 mm^3 after 14 d. However, the tumor volume of mice in free DOX, Lip@DOX and DOXDT groups was only increased to 595.97, 627.21 and 296.63 mm^3 , respectively. And the tumor volume of mice treated with DOXDT was obviously smaller than that of in another two groups. Hence, it concluded that DOXDT prodrug produced an obvious tumor suppression effect. Meanwhile, the body weight of mice treated with DOXDT prodrug was not obviously varied with the control group, indicating that DOXDT prodrug brought minimal damage to the health of mice. After the treatment of 14 d, tumors were excised from mice in different groups, which showed significant difference. The tumor size of mice in DOXDT treated group was the smallest among four groups, it was

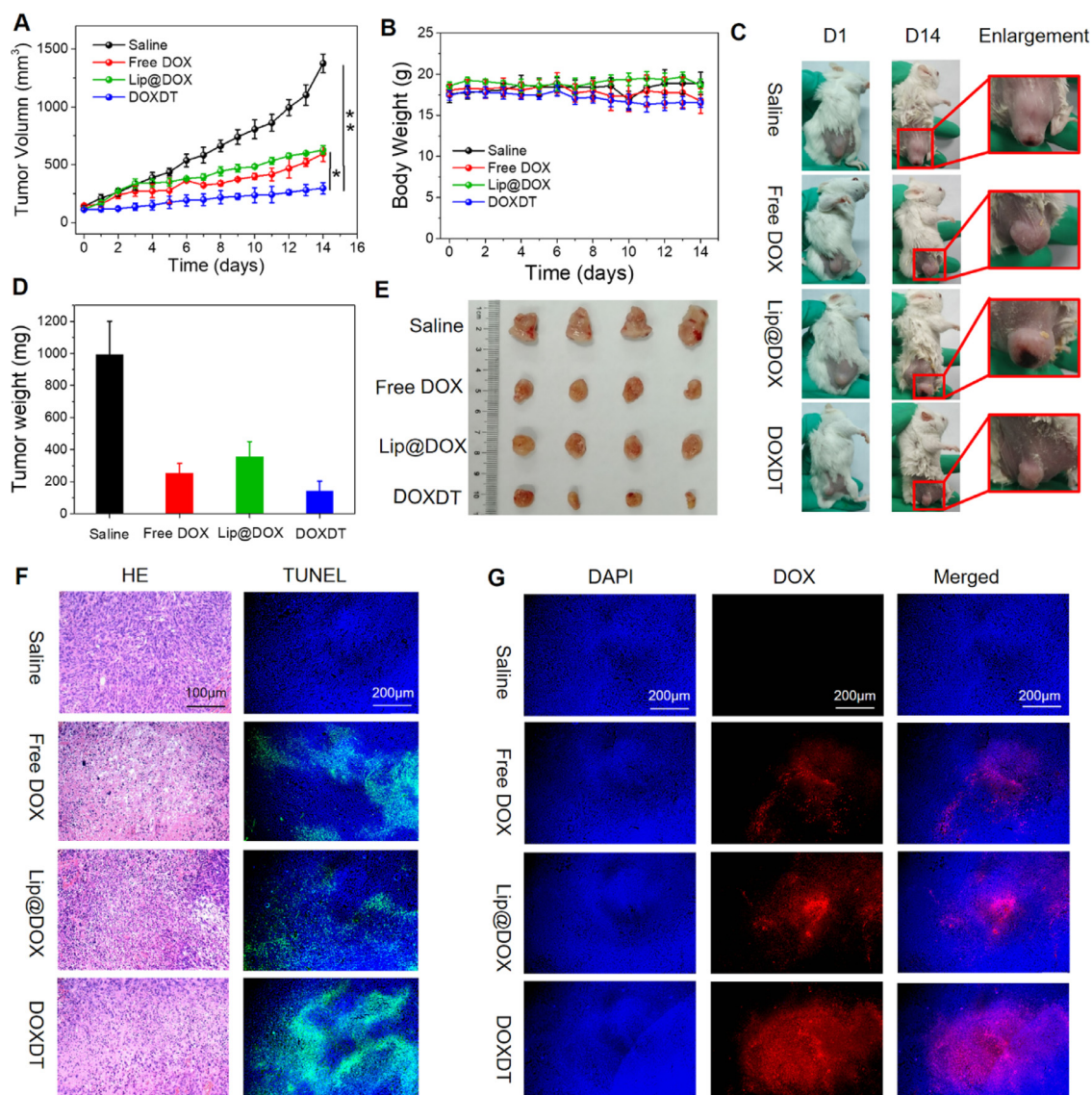


Fig. 5 – The *in vivo* therapeutic effects of DOXDT on tumors. Balb/C mice bearing 4T1 tumors treated with PBS, free DOX, Lip@DOX and DOXDT. The tumor volume (A) and body weight (B) were changed with time. (C) The Balb/C mice bearing 4T1 tumors at Day 1 and Day 14 (Data were reported as mean \pm SD ($n = 5$, * $P < 0.05$, ** $P < 0.01$). The weight (D) and images of off-body tumors (E). (F) The tumor was sliced and stained with H&E and TUNEL, respectively. (G) Tumor slices were stained with DAPI. Scale bars: 200 μ m.

followed by the mice in free DOX treated group (Fig. 5E). Above results proved that DOXDT prodrug had the highest tumor inhibition rate compared to the other three groups, up to 85.54%.

The tumor was sliced to further analyze the permeability of DOXDT for solid tumors [48]. The H&E staining of tumor slices verified the outstanding therapeutic efficacy of DOXDT (Fig. 5F). In DOXDT group, many the tumor cells were obviously impaired and the cell nucleus were destroyed. The drug-induced apoptosis in tumor tissues was further verified with TUNEL staining assay. As seen in Fig. 5F, the slices of tumors in DOXDT group showed the largest area of green fluorescence compared to that of in saline group, indicating the maximum apoptotic cells. The results of TUNEL and H&E showed that

DOXDT prodrug had a strong ability to promote the apoptosis of cancer cells.

The permeability of DOXDT in solid tumor was further studied by monitoring the distribution of red fluorescence of DOX in tumor slices. As showed in Fig. 5G, the strongest red fluorescence of DOX was observed in the tumor slices from DOXDT group, compared to free DOX and Lip@DOX groups. The results indicated that anti-cancer drug could be imported into solid tumors by the DOXDT prodrug, which may be resulted from the smaller size of DOXDT micelles. However, only a few red fluorescence signals of DOX were observed in the tumor slices in free DOX treated group, which could be due to the rapid clearance of free DOX in the body.

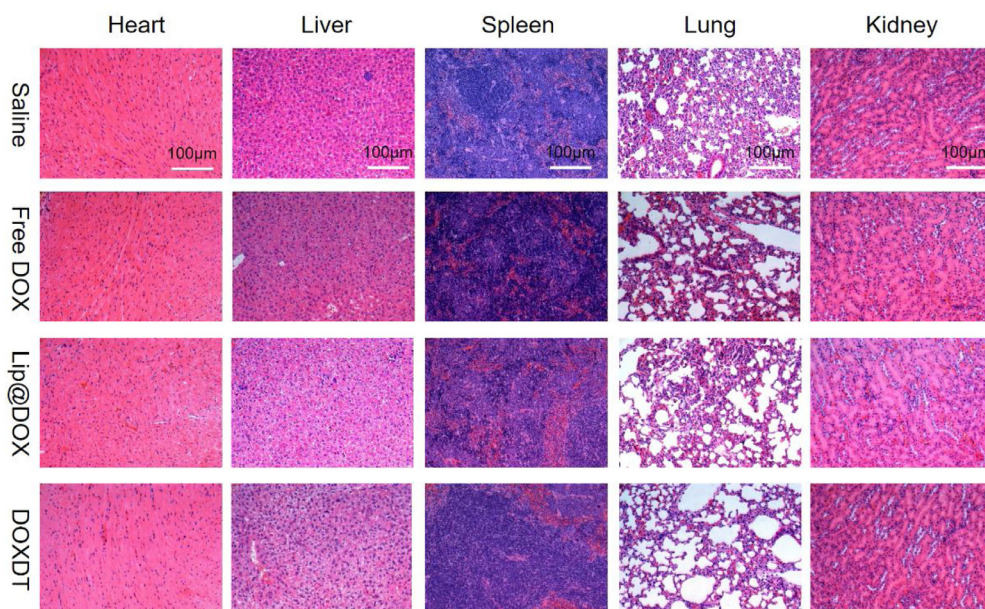


Fig. 6 – H&E staining of major organs of Balb/C mice. Scale bar: 100 µm.

In addition, the biosafety of DOXDT was assessed by the H&E staining of slices from major organs, including heart, liver, spleen, lung and kidney (Fig. 6). The results verified that DOXDT acidity-sensitive drug delivery system could effectively deliver DOX into tumor sites and anti-cancer drug DOX could be selectively accumulated in acid tumor environment, thus further enhancing anti-tumor therapeutic effects *in vivo*. Meanwhile, DOXDT prodrug presented minimal systemic toxicity to normal tissues. To sum up, DOXDT micelles might be the potential to open up a new avenue for clinical cancer treatment due to its good therapeutic ability and well *in vivo* biosafety.

4. Conclusion

In this study, an acidity-sensitive dextran-doxorubicin (DOXDT) prodrug was prepared with one-step ATRP. The amphiphilic prodrug can be formed into stable micelles. The prodrug showed several merits, including pH-sensitive DOX release, selectively drug accumulation in tumor, powerfully tumor permeability and cytotoxicity, as well as excellent biocompatibility. These significant advantages of DOXDT delivery system mainly attributed to its non-toxicity, good water-solubility, acidity-controlled release and small size of prodrug micelles. Importantly, DOXDT based delivery system remarkably enhanced the tumor suppressive efficiency, meanwhile exhibiting minimal systemic toxicity for normal tissues *in vivo* because of the acid-sensitive drug release behavior. This work provided a new strategy to enhance the therapeutic effects of chemotherapy drugs. This strategy is promising in the development translational DOX formulations, which would be widely applied in cancer therapy.

Conflicts of interest

The authors report no conflicts of interest. The authors alone are responsible for the content and writing of this article.

Acknowledgements

This study was supported by Science and Technology Project from the Science Technology and Innovation Committee of Shenzhen Municipality (JCY20170817170110940 and JCY20170307163529489), the Sichuan Science and Technology Program (2018JY0392 and 2018GZYZF0008), Sanming Project of Medicine in Shenzhen (SZSM201512033), and Shenzhen Public Service Platform of Molecular Medicine in Pediatric Hematology and Oncology.

Supplementary materials

Supplementary material associated with this article can be found, in the online version, at doi:10.1016/j.ajps.2019.10.001.

REFERENCES

- [1] Bray F, Ferlay J, Soerjomataram I, Siegel RL, Torre LA, Jemal A. Global cancer statistics 2018: GLOBOCAN estimates of incidence and mortality worldwide for 36 cancers in 185 countries. *CA Cancer J Clin* 2018;68:394–424.
- [2] Zhang Z, Yao J. Preparation of irinotecan-loaded folatargeted liposome for tumor targeting delivery and its antitumor activity. *AAPS PharmSciTech* 2012;13(3):802–10.

- [3] Zhang G, Liu F, Jia E, Zhang Y. Folate-modified, cisplatin-loaded lipid carriers for cervical cancer chemotherapy. *Drug Deliv* 2016;23(4):1393–7.
- [4] Maeda H, Khatami M. Analyses of repeated failures in cancer therapy for solid tumors: poor tumor-selective drug delivery, low therapeutic efficacy and unsustainable costs. *Clin Transl Med* 2018;7(1):11.
- [5] Soppimath SK, Aminabhavi TM, Kulkarni AR, Rudzinski WE. Biodegradable polymeric nanoparticles as drug delivery devices. *J Control Release* 2001;70(1–2):1–20.
- [6] Ling L, Ismail M, Du Y, Xia Q, He W, Yao C, et al. Reversible disulfide core-cross-linked multifunctional micelles for triggered release of camptothecin. *Mol Pharm* 2018;15(12):5479–92.
- [7] Wang S, Zhang J, Su H. Antitumor effect and toxicity of an albumin-paclitaxel nanocarrier system constructed via controllable alkali-Induced conformational. *ACS Biomater Sci Eng* 2019;5(4):1895–906.
- [8] Hare JL, Lammers T, Ashford MB, Puri S, Storm G, Barry ST. Challenges and strategies in anti-cancer nanomedicine development: an industry perspective. *Adv Drug Delivery Rev* 2017;108:25–38.
- [9] Al-Abd AM, Aljehani ZK, Gazzaz RW, Fakhri SH, Jabbad AH, Alahdal AM, et al. Pharmacokinetic strategies to improve drug penetration and entrapment within solid tumors. *J Control Release* 2015;219:269–77.
- [10] Choi IK, Strauss R, Richter M, Yun C, Lieber A. Strategies to increase drug penetration in solid tumors. *Front Oncol* 2013;3:193.
- [11] El-Sawy HS, Al-Abd AM, Ahmed TA, El-Say KM, Torchilin VP. Stimuli-responsive nano-architecture drug-delivery systems to solid tumor microenvironment: past, present, and future perspectives. *ACS Nano* 2018;12(11):10636–64.
- [12] Tong R, Cheng J. Anticancer polymeric nanomedicines. *Polym Rev* 2007;47(3):345–81.
- [13] Cheng Y, Qin S, Ma Y, Chen X, Zhang A, Zhang X. Super-pH-sensitive mesoporous silica nanoparticle-based drug delivery system for effective combination cancer therapy. *ACS Biomater Sci Eng* 2019;5(4):1878–86.
- [14] Gu D, Tan S, O'Connor AJ, Qiao G. On-demand cascade release of hydrophobic chemotherapeutics from a multicomponent hydrogel system. *ACS Biomater Sci Eng* 2018;4(5):1696–707.
- [15] Huang Y, Gao Y, Chen T, Xu Y, Lu W, Yu J, et al. Reduction-triggered release of CPT from acid-degradable polymeric prodrug micelles bearing boronate ester bonds with enhanced cellular uptake. *ACS Biomater Sci Eng* 2017;3(12):3364–75.
- [16] Ma G, Liu J, He J, Zhang M, Ni P. Dual-responsive polyphosphoester-doxorubicin prodrug containing a diselenide bond: synthesis, characterization and drug delivery. *ACS Biomater Sci Eng* 2018;4(7):2443–52.
- [17] Madea H. Enhanced permeability and retention (EPR) effect: basis for drug targeting to tumors in biomedical aspects of drug targeting. *Biomed Aspects Drug Targeting* 2002:211–28.
- [18] Natfji A, Ravishankar D, Osborn H, Greco F. Parameters affecting the enhanced permeability and retention effect: the need for patient selection. *J Pharm Sci* 2017;106(11):3179–87.
- [19] Golombek SK, May JN, Theek B, Appold L, Drude N, Kiessling F, et al. Tumor targeting via EPR: strategies to enhance patient responses. *Adv Drug Delivery Rev* 2018;130:17–38.
- [20] Guo Z, Li W, Yuan Y, Zheng K, Tang Y, Ma K, et al. Improvement of chemosensitivity and inhibition of migration via targeting tumor epithelial-to-mesenchymal transition cells by ADH-1-modified liposomes. *Drug Deliv* 2018;25(1):112–21.
- [21] Shen J, Kim H, Wolfram J, Mu C, Zhang W, Liu H, et al. A liposome encapsulated ruthenium polypyridine complex as a theranostic platform for triple-negative breast cancer. *Nano Lett* 2017;17(5):2913–20.
- [22] Jin Q, Deng Y, Chen X, Ji J. Rational design of cancer nanomedicine for simultaneous stealth surface and enhanced cellular uptake. *ACS Nano* 2019;13(2):945–77.
- [23] Hu J, Zhuang W, Ma B, Su X, Yu T, Li G, et al. Redox-responsive biomimetic polymeric micelle for simultaneous anticancer drug delivery and aggregation-induced emission active imaging. *Bioconjugate Chem* 2018;29(6):1897–910.
- [24] Bei R, Ghosh S. Glutathione triggered cascade degradation of an amphiphilic poly(disulfide)-drug conjugate and targeted release. *Bioconjugate Chem* 2019;30(1):101–10.
- [25] Xu M, Zhang C, Wu J, Zhou H, Bai R, Shen Z, et al. PEG-Detachable polymeric micelles self-assembled from amphiphilic copolymers for tumor-acidity-triggered drug delivery and controlled release. *ACS Appl Mater Interfaces* 2019;11(6):5701–13.
- [26] An X, Zhu A, Luo H, Ke H, Chen H, Zhao Y. Rational design of multi-stimuli-responsive nanoparticles for precise cancer therapy. *ACS Nano* 2016;10(6):5947–58.
- [27] Brega V, Scaletti F, Zhang X, Wang L, Li P, Xu Q, et al. Polymer amphiphiles for photoregulated anticancer drug delivery. *ACS Appl Mater Interfaces* 2019;11(3):2814–20.
- [28] Lin Y, Cheetham AG, Zhang P, Ou Y, Li Y, Liu G, et al. Multiwalled nanotubes formed by catanionic mixtures of drug amphiphiles. *ACS Nano* 2014;8(12):12690–700.
- [29] Kang M, Chakraborty K, Loverde S. Molecular dynamics simulations of supramolecular anticancer nanotubes. *J Chem Inf Model* 2018;58(6):1164–8.
- [30] Zhao Y, Zhao X, Chen Y, Guo X, Yuan W. Iron oxide nanoparticles-based vaccine delivery for cancer treatment. *Mol. Pharm* 2018;15(5):1791–9.
- [31] Coleman BR, Moffitt MG. Amphiphilic inorganic nanoparticles with mixed polymer brush layers of variable composition: bridging the paradigms of block copolymer and nanoparticle self-assembly. *Chem Mater* 2018;30(7):2474–82.
- [32] Yoon HY, Jeon S, You D, Park J, Kwon IC, Koo H, et al. Inorganic nanoparticles for image-guided therapy. *Bioconjugate Chem* 2017;28(1):124–34.
- [33] Falagan-Lotsch P, Grzincic EM, Murphy CJ. New advances in nanotechnology-based diagnosis and therapeutics for breast cancer: an assessment of active-targeting inorganic nanoplatfoms. *Bioconjugate Chem* 2017;28(1):135–52.
- [34] Lammers L, Kiessling K, Hennink WE, Storm G. Drug targeting to tumors: principles, pitfalls and (pre-) clinical progress. *J Control Release* 2012;161(2):175–87.
- [35] Björnalm M, Thurecht KJ, Michael M, Scott AM, Caruso F. Bridging bio-nano science and cancer nanomedicine. *ACS Nano* 2017;11(10):9594–613.
- [36] Shi X, Hou M, Bai S, Ma X, Gao Y, Xiao B, et al. Acid-activatable theranostic unimolecular micelles composed of amphiphilic star-like polymeric prodrug with high drug loading for enhanced cancer therapy. *Mol Pharma* 2017;14(11):4032–41.
- [37] Thapa P, Li M, Bio M, Rajaputra P, Nkepan G, Sun Y, et al. Far-red light-activatable prodrug of paclitaxel for the combined effects of photodynamic therapy and site-specific paclitaxel chemotherapy. *J Med Chem* 2016;59(7):3204–14.
- [38] Liu L, Qiu W, Li B, Zhang C, Sun L, Wan S, et al. A dual-FRET-based versatile prodrug for real-time drug release monitoring and in situ therapeutic efficacy evaluation. *Adv Funct Mater* 2015;25:7317–26.

- [39] Bai S, Gao Y, Ma X, Shi X, Hou M, Xue P, et al. Reduction-active polymeric prodrug micelles based on α -cyclodextrin polyrotaxanes for triggered drug release and enhanced cancer therapy. *Carbohydr Polym* 2018;193:153–62.
- [40] Song S, Shi Y, Zhang L, Hu H, Zhang C, Yin M, et al. Synthesis of CSK-DEX-PLGA nanoparticles for the oral delivery of exenatide to improve its mucus penetration and intestinal absorption. *Mol Pharma* 2019;16(2):518–32.
- [41] Shi X, Ma X, Hou M, Gao Y, Bai S, Xiao B, et al. pH-Responsive unimolecular micelles based on amphiphilic star-like copolymers with high drug loading for effective drug delivery and cellular imaging. *J Mater Chem B* 2017;5:6847–59.
- [42] Jin X, Tong G, Zhu X. Star polymer-based unimolecular micelles and their application in bio-imaging and diagnosis. *Biomaterials* 2018;178:738–50.
- [43] Wang H, Xu F, Li D, Liu X, Jin Q, Ji J. Bioinspired phospholipid polymer prodrug as a pH-responsive drug delivery system for cancer therapy. *Polym Chem* 2013;4:2004–10.
- [44] Tang Q, Xiao W, Huang C, Si W, Shao J, Huang W, et al. pH-Triggered and enhanced simultaneous photodynamic and photothermal therapy guided by photoacoustic and photothermal imaging. *Chem Mater* 2017;29:5216–24.
- [45] Chen H, Fan J, Zhao L, Fan G, Zheng R, Qiu X, et al. Chimeric peptide engineered exosomes for dual-stage light guided plasma membrane and nucleus targeted photodynamic therapy. *Biomaterials* 2019;211:14–24.
- [46] Liu F, Cong Y, Qi G, Ji L, Qiao Z, Wang H. Near-infrared laser driven in situ self-assembly as a general strategy for deep tumor therapy. *Nano Lett* 2018;18(10):6577–84.
- [47] Zhou Q, Shao S, Wang J, Xu C, Xiang J, Piao Y, et al. Enzyme-activatable polymer–drug conjugate augments tumour penetration and treatment efficacy. *Nat Nanotechnol* 2019;14:799–809.
- [48] Zhang P, Wang J, Chen H, Zhao L, Chen B, Chu C, et al. Tumor microenvironment-responsive ultrasmall nanodrug generators with enhanced tumor delivery and penetration. *J Am Chem Soc* 2018;140(44):14980–9.